


Article

An Improved WMS-2f/1f Spectral Fitting Method Using Orthogonal Test in Initial Parameters Selection

Liezhao Luo ^{1,2}, Ting Li ^{1,2,*}, Jiangge Deng ^{1,2} , Runzhou Zhao ^{1,2} and Jinkui Wang ^{1,2}

¹ School of Energy and Power Engineering, Beihang University, Beijing 100191, China

² National Key Laboratory of Science and Technology Aero-Engine Aero-Thermodynamics, Beihang University, Beijing 102206, China

* Correspondence: li1329@buaa.edu.cn

Abstract: This paper proposes an improved wavelength modulation spectroscopy with the 2nd harmonics normalized by the 1st harmonics (WMS-2f/1f) spectral fitting method using the orthogonal test in selection of the initial parameters. The method is implemented and validated experimentally in measurement of the temperature of diluted H₂O in air (1 atm, 291K, 0.7%) by the WMS-2f/1f technique. The transition center wavelength targets near 1344 nm. Results demonstrate that the sum-square-error (SSE) between the calculated and measured WMS-2f/1f spectral profiles decreases significantly within given updating times when the optimized initial parameters are used. Compared to the conventional method, the optimized initial parameters can make the fitting routine converge more efficiently. The temperature of the vapor inferred from the proposed spectral fitting method are in good agreement with the true values.

Keywords: TDLAS; wavelength modulation spectroscopy; orthogonal test; spectral fitting



Citation: Luo, L.; Li, T.; Deng, J.; Zhao, R.; Wang, J. An Improved WMS-2f/1f Spectral Fitting Method Using Orthogonal Test in Initial Parameters Selection. *Sensors* **2022**, *22*, 7430. <https://doi.org/10.3390/s22197430>

Academic Editor: Anna Chiara De Luca

Received: 22 August 2022

Accepted: 27 September 2022

Published: 30 September 2022

Publisher's Note: MDPI stays neutral with regard to jurisdictional claims in published maps and institutional affiliations.



Copyright: © 2022 by the authors. Licensee MDPI, Basel, Switzerland. This article is an open access article distributed under the terms and conditions of the Creative Commons Attribution (CC BY) license (<https://creativecommons.org/licenses/by/4.0/>).

1. Introduction

The tunable diode laser absorption spectroscopy (TDLAS) has drawn considerable attention in the last few decades. Due its high sensitivity, accuracy and non-intrusive characteristics, it has been applied in various fields [1–13]. The TDLAS techniques can be categorized into direct absorption spectroscopy (DAS) and wavelength modulation spectroscopy (WMS). The former is relatively straight forward but susceptible to the harsh environment. The latter is complicated in the theory and data process but it can achieve improved noise-rejection ability and sensitivity [14]. In WMS, the laser is scanned by a low-frequency waveform f_s and a high-frequency sinusoidal waveform f_m simultaneously. Therefore, the absorption information is conveyed to the high frequency harmonics. In order to decouple the absorption information from harmonics, several strategies have been developed [15–22]. Among them, the scanned-WMS- $nf/1f$ fitting method proposed by Sun et al. [19] and developed by Goldenstein et al. [14] is effective for all kinds of situations and avoids the complex analytic expression [16,18], which makes it prevail in the WMS data process. In this scheme, the absorption information is retrieved from harmonics by fitting the simulated WMS- $nf/1f$ spectral profile to the measured one proceeded with the same digital lock-in amplifier. Specifically, the spectral parameters, such as the integrated absorbance area, A , the transition center frequency, ν_0 and the lineshape width, $\Delta\nu$, are used as the free values in the fitting routine. If the sum-square-errors (SSE) between the simulated WMS- $nf/1f$ profile and the measured one reach to the predetermined value, the outputs of the routine are employed to infer the gas properties. Nevertheless, it may take a long time to obtain the satisfied results when the initial parameters are chosen inappropriately, for the efficiency of the fitting routine is heavily dependent on the values of initial parameters. However, the investigation of the initial parameter optimization in the WMS- $nf/1f$ fitting is rather limited.

The orthogonal test method (OTM) is based on the orthogonal table to analyze the experiment results scientifically [23]. It has been applied widely in optimizing the experimental scheme, which can reduce testing numbers, shorten test time and minimize cost [24–28]. In this study, the WMS- $\eta f/1f$ fitting performance is dependent on the initial parameters, namely the integrated absorbance area, A , the transition center frequency, and ν_0 , the lineshape width, $\Delta\nu$, which is similar to the multifactor and multilevel problem in the orthogonal test method. Therefore, it is possible to optimize the initial parameters with the orthogonal test method to enhance the fitting efficiency.

In this paper, the optimization of initial parameters was performed based on the orthogonal test method. The optimized initial parameters were used to match the measured WMS- $2f/1f$ spectral to infer the gas properties, which decreased the SSE between the calculated WMS- $2f/1f$ spectral profile and the measured one within the given updating times and shortened the fitting period, accordingly, enhancing the fitting routine efficiency.

2. Theory

2.1. Wavelength Modulation Spectroscopy

The basic principle of WMS has been described in detail in large quantities of other literature [29–32]. Here, a brief review is presented. All the absorption spectroscopy techniques are governed by the Beer-Lambert law that relates the transmitted and the incident light at frequency, ν , as described in Equation (1)

$$I_{t,\nu} = I_{0,\nu} \exp(-\alpha_\nu) = I_{0,\nu} \exp(-S(T)\phi_\nu P X_{abs} L) \quad (1)$$

where $I_{t,\nu}$ and $I_{0,\nu}$ are transmitted and incident light intensity at frequency, ν , respectively. α_ν is the spectral absorption at frequency ν . $S(T)$ ($\text{cm}^{-2}\text{atm}^{-1}$) is the line strength, which is dependent on temperature only. P (atm) is the total pressure of the absorbing species and X_{abs} is the mole fraction of the absorbing species. ϕ_ν represents the line shape function and L (cm) is the optical length.

WMS is an advanced TDLAS technique based on direct absorption spectroscopy (DAS), which has a higher signal noise ratio (SNR) and is more suitable for the hostile environment compared to DAS. When the current is injected into the DFB laser with a low frequency and a high frequency sinusoidal waveform, the intensity of the laser, $I_0(t)$, and the frequency of the laser, $\nu(t)$, can be modeled using Equations (2) and (3), [14] respectively.

$$I_0(t) = \bar{I}_0(1 + i_{1,s} \sin(2\pi f_s t + \varphi_{1,s}) + i_{2,s} \sin(4\pi f_s t + \varphi_{2,s}) + i_{1,m} \sin(2\pi f_m t + \varphi_{1,m}) + i_{2,m} \sin(4\pi f_m t + \varphi_{2,m})) \quad (2)$$

$$\nu(t) = \bar{\nu}_0 + a_{1,s} \sin(2\pi f_s t + \varnothing_{1,s}) + a_{2,s} \sin(4\pi f_s t + \varnothing_{2,s}) + a_{1,m} \sin(2\pi f_m t + \varnothing_{1,m}) + a_{2,m} \sin(4\pi f_m t + \varnothing_{2,m}) \quad (3)$$

Here, the subscripts s and m represent the characteristic changes of intensity or frequency due to the scan and modulation, respectively. \bar{I}_0 is the mean intensity; i_1 and i_2 are the first- and second-order mean-normalized intensity amplitude, respectively; f [Hz] is the user-specified frequency; φ_1 and φ_2 are the absolute phase shift of the first- and second-order intensity; similarly, \varnothing_1 and \varnothing_2 are the absolute phase shift of the first- and second-order frequency; $\bar{\nu}_0$ (cm^{-1}) is the center optical frequency of the laser. a_1 and a_2 [cm^{-1}] are the first- and second-order scan or modulation depth.

The low frequency current scans the majority of absorption lineshape, while the high frequency modulation current transfers the absorption information to the harmonics. In order to acquire absorption information from harmonics, the most widely used method is the 2nd harmonics normalized by 1st harmonics, namely WMS- $2f/1f$. In this study, the harmonics were obtained using the approach presented by Goldenstein et al. [14]. The transmitted light signal is multiplied by a reference cosine and sine wave at $2f_m$, respectively, which are then passed through the low-pass filter to obtain the corresponding $X_{2f}(t)$ and $Y_{2f}(t)$ components. The $X_{1f}(t)$ and $Y_{1f}(t)$ can be obtained in a similar way, where

the frequency of the reference signal is changed to $1f_m$. The WMS- $2f/1f$ signal intensity can be calculated by eq.4, which is a function of the integrated absorbance area, lineshape function and laser characteristics [14].

$$WMS_{2f/1f}(t) = \sqrt{X_{2f}^2(t) + Y_{2f}^2(t)} / \sqrt{X_{1f}^2(t) + Y_{1f}^2(t)} \quad (4)$$

In this scheme, the transition center frequency (ν_0), the integrated absorbance area (A) and the lineshape width ($\Delta\nu$) are employed as free parameters to fit the simulated WMS- $nf/1f$ spectral profile to the measured one. The iteration fitting routine is shown in Figure 1. When the minimum sum-of-squared errors (SSE) between the simulation and measured WMS- $2f/1f$ meet the user-specified requirement, the best fitting parameters are employed to determine the gas property. An intelligent guess for initial parameters would reduce the update times dramatically. However, it is difficult to obtain the intelligent guesses for the fitting routine when under an unknown circumstance. The less you know about the measurement situation, the harder you acquire appropriate guesses. One should note that the lineshape width should be dependent on both the collisional width and Doppler width. Nevertheless, in order to reduce the fitting complexity, only the collisional width is floated and the Doppler width is fixed at a given temperature. If the inferred gas temperature deviates far away from the given temperature, an iteration between Doppler width and fitting procedure may be needed.

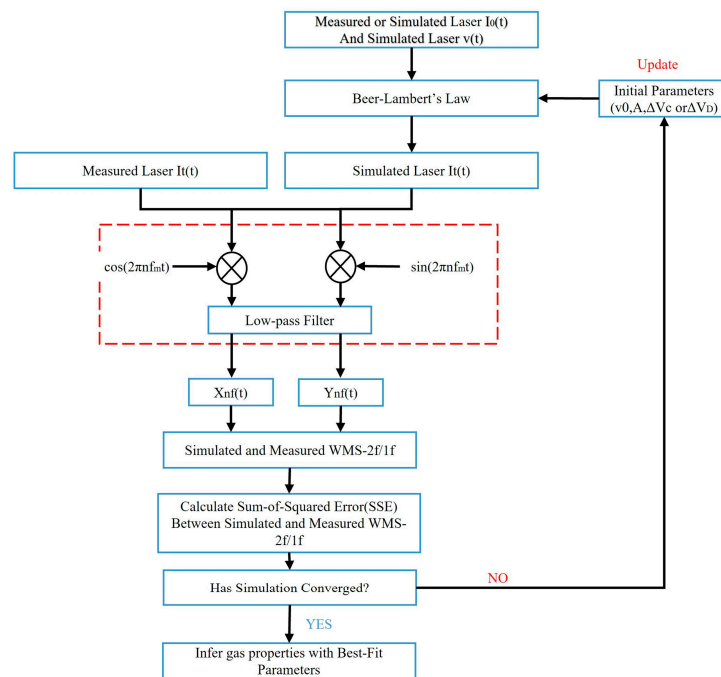


Figure 1. Flow chart of scanned-WMS- $2f/1f$ spectral fitting routine. The guess values of initial parameters are firstly employed in the iteration. If the SSE is smaller than the predetermined value when the iteration converges, the outputs of the iteration are used to infer gas properties. Otherwise, the initial parameters have to be updated and repeat the iteration.

2.2. Orthogonal Test Method

Orthogonal test method (OTM) is used to study several factors and levels. Based on the appropriate orthogonal table, it can conduct tests with optimum parameters to reduce test times and curtail the test period. The factors are referred to the parameters which influence the final result in a specified experiment, while the levels are equal to the maximum number of the values that any single factor can be set as [26].

In this study, the WMS- $2f/1f$ spectral profile is affected by the initial values, namely the integrated absorbance area (A), center frequency (ν_0) and collisional width ($\Delta\nu_c$). If

the initial values are chosen inappropriately, the final value of SSE may not satisfy the requirement of the predetermined SSE after a certain amount of iteration, even though the iteration converges. Sequentially the initial values have to be updated and the iteration process is repeated to meet the requirement. Normally, the farther the initial parameters deviate from the true gas properties, the more times they need updated, which is time-consuming and puts challenge to the hardware device. On the contrary, when the improved initial values are employed, it can decrease the initial-parameters-updating times and consequently curtail the period of the fitting routine.

Therefore, the A , ν_0 and $\Delta\nu_c$ are set as three factors in an orthogonal experiment to determine the optimal initial values. The levels of each parameter are selectively some typical values of parameters according to specific conditions. In this study, the three levels of A are 0.001, 0.002 and 0.003. The three levels of ν_0 are 7444.35, 7444.37 and 7444.39 cm^{-1} . Those of $\Delta\nu_c$ are selected as 0.02, 0.05 and 0.08 cm^{-1} . All the factors of levels are decided by roughly calculating, and are not required to be specific. The chosen factors and their corresponding levels are shown in Table 1.

Table 1. The factors and levels in the Orthogonal Test.

Factors	Integrated Absorbance Area (A)	Center Frequency (ν_0) [cm^{-1}]	Collisional Width ($\Delta\nu_c$) [cm^{-1}]
Level 1	0.001	7444.35	0.02
Level 2	0.002	7444.37	0.05
Level 3	0.003	7444.39	0.08

3. Experimental Validation

The schematic of the experimental setup is shown in Figure 2. To validate the performance of the optimized initial parameters determined by OTM, a DFB tunable diode laser (NEL) near 1343 nm was used to probe the vapor temperature based on scanned-WMS- $2f/1f$ at room temperature (291K, 1 atm). The H_2O mole fraction was 0.7% measured by a hygrometer. A function generator (RIGOL 4102) controlled by the LabVIEW was used to produce a slow sinusoidal waveform ($f_s = 100$ Hz) and a fast one ($f_m = 10$ kHz). The combined waveform was then delivered to a laser controller (Arroyo 6305), which can change the output intensity and wavelength of a DFB laser via temperature and current. The light from the laser passed through the test region, whose optical length (L) was 137 cm and was directed upon the detector (Thorlabs, PDA20CS2). The transmitted signal was recorded by a USB DAQ (NI 9223) with a 1 Msa/s sampling rate. The raw signal was then processed in a computer to obtain the measured harmonics' signals. It must have been mentioned that the frequency characteristics ($\nu(t)$) of this laser has been conducted prior to the experiment.

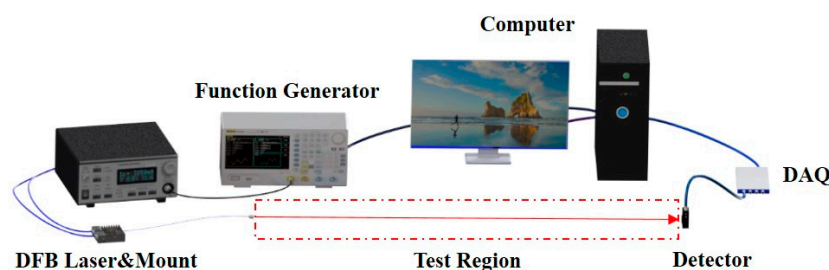


Figure 2. The schematic of the experimental setup.

4. Results and Discussions

4.1. Optimized Initial Parameters Obtained by OTM

The partially raw signal and two typical sets of WMS- $2f/1f$ spectral profiles are shown in Figure 3. Although the absorption of H_2O is very weak in the room condition, the vapor

properties can also be inferred from the WMS- $2f/1f$ profile with the strategy introduced in Section 2.1.

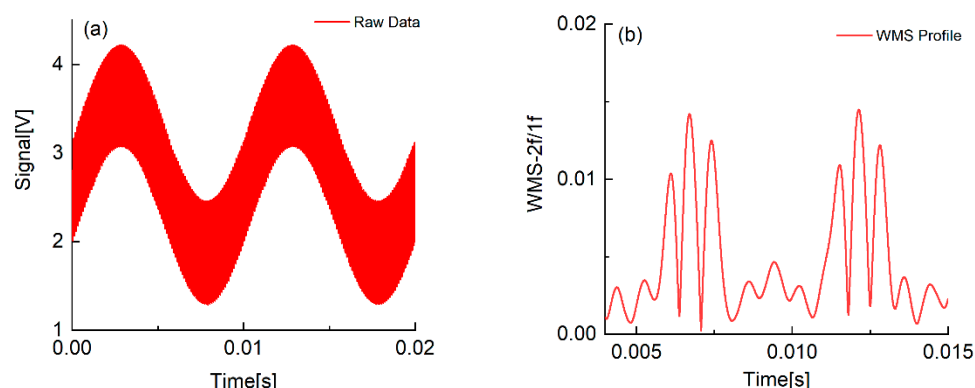


Figure 3. The raw detected signal (a) and the corresponding WMS- $2f/1f$ spectral profile (b).

To gain the optimized initial parameters and shorten the fitting routine period, a parameter-optimization procedure based on OTM using orthogonal table $L_9(3^4)$ was performed. Since the goodness of fitting between the simulated and measured WMS- $2f/1f$ profile is indicated by the SSE, it is appropriate to employ the value of SSE to evaluate the fitting performance of different initial parameters after the given updating times. The different combinations of three factors with three levels (in Table 1) based on the orthogonal table were used as the initial parameters to fit the measured WMS- $2f/1f$ profile, and the minimal SSE was calculated after the initial parameters updated 50 times, as shown in Table 2. In the fitting routine, the Levenberg-Marquardt algorithm was employed. It is obvious that the values of SSE vary dramatically with different initial parameters. The bigger the value is, the worse is the fitting performance. Moreover, it is necessary to update the initial parameters with more times to obtain satisfactory results. Take the test 8 for example; the value of SSE is as high as 0.9561091, which indicates the fitting effect is not satisfying. Therefore, the initial parameters of test 8 have to be updated with more times to improve the fitting performance.

Table 2. Orthogonal Array $L_9(3^4)$ and the SSE.

Test Numbers	Factors			SSE
	Integrated Absorbance Area (A)	Center Frequency (ν_0) (cm^{-1})	Collisional Width ($\Delta\nu_c$) (cm^{-1})	
1	0.001	7444.35	0.02	0.0106581
2	0.001	7444.37	0.05	0.0015216
3	0.001	7444.39	0.08	0.0042488
4	0.002	7444.35	0.05	0.0034304
5	0.002	7444.37	0.08	0.0043295
6	0.002	7444.39	0.02	0.0602594
7	0.003	7444.35	0.08	0.7740496
8	0.003	7444.37	0.02	0.9561091
9	0.003	7444.39	0.05	0.8002515

It necessitates further analysis of the orthogonal test results to locate the optimal initial parameters via range analysis. Range analysis is a statistical method to determine the factors' sensitivity to the experimental result according to the orthogonal experiment. Range is defined as the distance between the extreme values of the data. The greater the range is, the more sensitive is the factor [33]. The summation of SSE from i -level for a specific

x -factor, K_i^x , the average of K_i^x , k_i^x , and the range, R^x , is calculated by Equations (5)–(7) [28], respectively. The results are listed in Table 3.

$$K_i^x = \sum SSE \text{ from the level } i \text{ and factor } x \quad (5)$$

$$k_i^x = K_i^x / 3 \quad (6)$$

$$R^x = \max(k_1^x, k_2^x, k_3^x) - \min(k_1^x, k_2^x, k_3^x) \quad (7)$$

Table 3. Analysis of the orthogonal results.

	Factors		
	Integrated Absorbance Area (A)	Center Frequency (ν_0) (cm ⁻¹)	Collisional Width ($\Delta\nu_c$) (cm ⁻¹)
K_1^x	0.016429	0.788138	1.027027
K_2^x	0.068019	0.961960	0.805204
K_3^x	2.530410	0.864760	0.782628
k_1^x	0.005476	0.262713	0.342342
k_2^x	0.022673	0.320653	0.268401
k_3^x	0.843470	0.288253	0.260876
R^x	0.837994	0.057940	0.081466

According to the value of R in Table 3, it can be concluded that the SSE, namely, the performance of fitting, is primarily affected by the initial value of the integrated absorbance area among the three factors. However, it is reminded that the effects of the other two factors cannot be ignored. From the data in Table 3, it can be found that $k_1^A < k_2^A < k_3^A$, $k_1^{\nu_0} < k_3^{\nu_0} < k_2^{\nu_0}$ and $k_3^{\Delta\nu_c} < k_2^{\Delta\nu_c} < k_1^{\Delta\nu_c}$. This result implies that the optimal initial parameters are the combination of the integrated absorbance area, A, with Level 1, center frequency, ν_0 , with Level 1 and collisional width, $\Delta\nu_c$, with Level 3, namely, 0.001, 7444.35 and 0.08 cm⁻¹, respectively.

4.2. Fitting Performance of the Optimized Initial Parameters

With the optimized initial parameters obtained above, the fitting routine can meet the SSE requirement within less initial parameter-updating times and improve the fitting efficiency. To illustrate this benefit, 20 sets of random values around the optimized initial parameters and 20 sets of random initial parameters in the range from 0.001 to 0.003 for A, 7444.35 to 7444.37 cm⁻¹ for ν_0 and 0.02 to 0.08 cm⁻¹ for $\Delta\nu_c$ were used to match the same measured WMS-2f/1f spectral profile. All the initial parameters were allowed to be updated no more than 50 times, and their respective minimal SSE were calculated. The final results are shown in Figure 4.

In this figure, the blue diamond indicates the minimal SSE of the fitting by the optimized initial parameters obtained with OTM, while the red ones represent the minimal SSE of the fitting by random initial parameters. In Figure 4a, it is apparent that all the minimal SSEs from the optimized parameters are buried in the gray layer. By contrast, the majority of the minimal SSEs from random initial parameters are outside the gray region. This characteristic implies that the optimized initial parameters obtained from the OTM can reach a smaller SSE in given updating times compared with the random ones. Furthermore, if the user-specified SSE is 0.0025, all the SSEs from optimized initial parameters can meet the requirement. However, only three sets of random initial parameters' SSEs are smaller than the required SSE, as shown in Figure 4b. It means that those initial parameters, which do not satisfy the requirement, need more times to update their values.

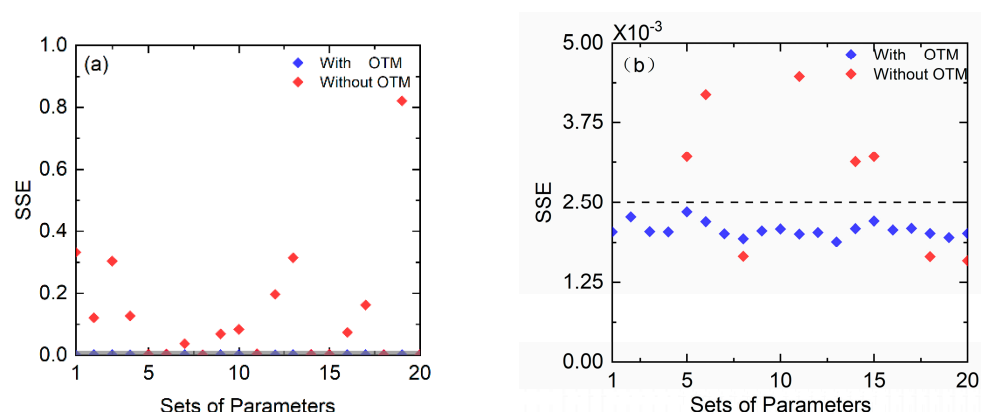


Figure 4. (a) The values of SSE between the simulated and measured WMS- $2f/1f$ spectral profile. The red diamond indicates the minimal SSE of the fitting by the optimized initial parameters obtained from the orthogonal test method, while the red ones represent the minimal SSE of the fitting by random initial parameters. (b) presents the zoomed in view of the gray region in (a). It is evident that all the SSE from the optimized initial parameters are less than 0.0025, while it is only 3 sets for random initial parameters, as shown in (b).

Theoretically, as long as the initial parameters are updated frequently enough, they eventually can meet the SSE requirement to converge the fitting routine, no matter which values the initial parameters takes. However, it is rather time-consuming. To illustrate this characteristic visually, 100 sets of initial parameters were selected randomly around the optimized values obtained by OTM and from the same range as above, respectively, all of which were applied to match the same measured WMS- $2f/1f$ spectral profile. As the Figure 5 shows, the blue bar represents the distribution of time the near optimized initial parameters took, and the red is the distribution of time cost by the unimproved initial parameters. It is obvious that the majority of the optimized parameters took less than 20 s to converge the fitting routine, accounting for near 80%. More specifically, many of them took even less than 5 s and no one was found beyond 60 s. Nevertheless, when fitting with the parameters without optimization, nearly 90% of the sets cost more than 50 s to obtain the same results. In addition, the sets of parameters costing below 20 s accounted for less than one fifth. The averagely consumed time with the optimized initial parameters was 10.3 s, while it was 49.5 s for the parameters without optimization, near 5 times longer than the former. Therefore, the optimized initial parameters can effectively curtail the period of fitting routine and accelerate gas property inference from the WMS- $2f/1f$ spectral profile, which is helpful, especially when faced with a large amount of fitting data.

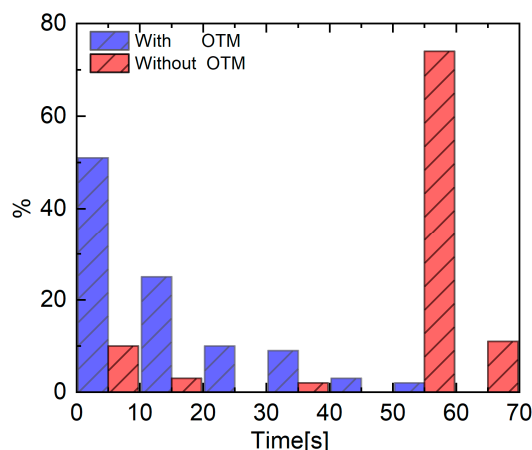


Figure 5. The time distribution comparison of the optimized initial parameters and the unimproved ones to fit the same measured WMS- $2f/1f$ spectral profile.

4.3. Temperature from the WMS-2f/1f

Figure 6a presents a single-scan measured WMS-2f/1f spectral profile of the H₂O transition near 7444.35 cm^{−1} and the corresponding best-fit with the optimized initial parameters. In all fitting routines, $\Delta\nu_D$ was fixed at the value given by the known temperature and A , ν_0 and $\Delta\nu_c$ were free parameters obtained by OTM. The simulated WMS-2f/1f spectral agrees well with the whole measurement. However, there exists a visible difference in the region of the left lobe, which may be caused by the low absorbance as stated in Section 4.1. However, this deviation does not influence the final gas property inference too much.

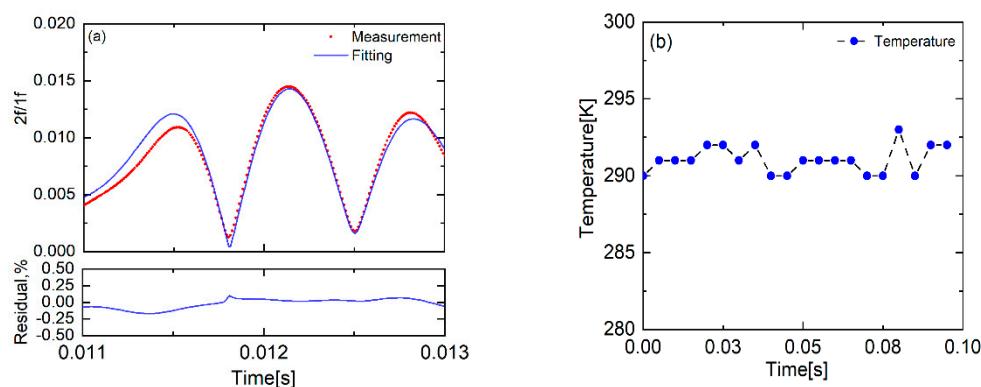


Figure 6. (a) The measured and the best-fit WMS-2f/1f spectral profile. (b) The inferred temperature in room conditions by the WMS-2f/1f strategy.

The integrated absorbance area from the scanned-WMS-2f/1f spectral fitting routine was used to deduce the vapor temperature with the known H₂O mole fraction, 0.7%, measured by a hygrometer. Figure 6b shows the inferred temperature during 10 scan-cycles of the laser, namely 0.1 s. The WMS-2f/1f measured temperature was in good agreement with the value measured by K type thermocouple (291K). The slight variation of the WMS-2f/1f measured temperature was reasonable. The measurement uncertainty originates primarily from the fitting residual (<0.25% from Figure 6a), the hygrometer (~1%) and the reference linestrength (~2%) [34]. Therefore, the measured temperature uncertainty was about 2.25%. Note that the laser was scanned by a sinusoidal waveform with 100 Hz, so there existed absorption when scanned up or down in one cycle. Therefore, the measurement temporal resolution was increased to 200 Hz.

5. Conclusions

A strategy based on the orthogonal test method is proposed to optimize the initial parameters of the scanned-WMS-2f/1f spectral fitting routine. With the optimized initial parameters, the sum-of-squared errors (SSE) between the simulated and measured WMS-2f/1f profile can be greatly reduced in the given initial-parameters-updated times. Consequently, the fitting routine converges more efficiently. As stated before, on average, it took about 10 s to make the fitting routine converge with the optimized initial parameters. Meanwhile it needed 50 s to obtain the same results using the conventional method. When faced with a large amount of fitting data, it can save roughly 80% calculating time using this novel method. The measurement of gas temperature was performed by WMS in the controlled condition ($T = 291\text{K}$, $X_{\text{abs}} = 0.7\%$, $P = 1\text{ atm}$). Moreover the inferred temperature with the optimized initial parameters was consistent with the controlled value.

Author Contributions: Conceptualization, L.L. and T.L.; methodology, L.L.; software, L.L. and J.D.; investigation, L.L., R.Z. and J.W.; writing—original draft preparation, L.L.; writing—review and editing, T.L.; visualization, all authors.; supervision, T.L.; project administration, L.L. and T.L.; funding acquisition, T.L. All authors have read and agreed to the published version of the manuscript.

Funding: This research was funded by National Natural Science Foundation of China (Grant No. 61827802), and the State Key Laboratory of High Temperature Gas Dynamics (Grant No. 2021KF05).

Institutional Review Board Statement: Not applicable.

Informed Consent Statement: Not applicable.

Data Availability Statement: The data presented in this study are available on request from the corresponding author.

Conflicts of Interest: The authors declare no conflict of interest.

References

1. Webber, M.E.; Baer, D.S.; Hanson, R.K. Ammonia monitoring near 1.5 μm with diode-laser absorption sensors. *Appl. Opt.* **2001**, *40*, 2031–2042. [[CrossRef](#)] [[PubMed](#)]
2. Zhang, G.; Liu, J.; Xu, Z.; He, Y.; Kan, R. Characterization of temperature non-uniformity over a premixed CH₄-air flame based on line-of-sight TDLAS. *Appl. Phys. B* **2016**, *122*, 3. [[CrossRef](#)]
3. So, S.; Jeong, N.; Song, A.; Hwang, J.; Lee, C. Measurement of temperature and H₂O concentration in premixed ch₄/air flame using two partially overlapped H₂O absorption signals in the near infrared region. *Appl. Sci.* **2021**, *11*, 3701. [[CrossRef](#)]
4. McGettrick, A.J.; Duffin, K.; Johnstone, W.; Stewart, G.; Moodie, D.G. Tunable diode laser spectroscopy with wavelength modulation: A phasor decomposition method for calibration-free measurements of gas concentration and pressure. *J. Light. Technol.* **2008**, *26*, 432–440. [[CrossRef](#)]
5. Ahmed, F.; Esmail, M.; Kawahara, N.; Tomita, E. CO₂ concentration measurements inside expansion-compression engine under high EGR conditions using an infrared absorption method. *Ain Shams Eng. J.* **2019**, *11*, 787–793. [[CrossRef](#)]
6. Li, H.; Farooq, A.; Jeffries, J.B.; Hanson, R.K. Diode laser measurements of temperature-dependent collisional narrowing and broadening parameters of Ar-perturbed H₂O transitions at 1391.7 and 1397.8 nm. *J. Quant. Spectrosc. Radiat. Transf.* **2008**, *109*, 132–143. [[CrossRef](#)]
7. Goldenstein, C.S.; Spearrin, R.M.; Jeffries, J.B.; Hanson, R.K. Infrared laser-absorption sensing for combustion gases. *Prog. Energy Combust. Sci.* **2017**, *60*, 132–176. [[CrossRef](#)]
8. Luo, L.; Li, T.; Deng, J.; Zhao, R.; Wang, J.; Xu, L. Experimental Investigation on Self-Excited Thermoacoustic Instability in a Rijke Tube. *Appl. Sci.* **2022**, *12*, 8046. [[CrossRef](#)]
9. Reuter, S.; Sousa, J.S.; Stancu, G.D.; van Helden, J.H. Review on VUV to MIR absorption spectroscopy of atmospheric pressure plasma jets. *Plasma Sources Sci. Technol.* **2015**, *24*, 054001. [[CrossRef](#)]
10. Wei, M.; Kan, R.; Chen, B.; Xu, Z.; Yang, C.; Chen, X.; Xia, H.; Hu, M.; He, Y.; Liu, J.; et al. Calibration-free wavelength modulation spectroscopy for gas concentration measurements using a quantum cascade laser. *Appl. Phys. B* **2017**, *123*, 149. [[CrossRef](#)]
11. Witzel, O.; Klein, A.; Meffert, C.; Wagner, S.; Ebert, V. Vcsel-based, high-speed, in situ TDLAS for in-cylinder water vapor measurements in IC engines. *Opt. Express* **2013**, *21*, 19951–19965. [[CrossRef](#)] [[PubMed](#)]
12. Goldenstein, C.S.; Jeffries, J.B.; Hanson, R.K. Diode laser measurements of line strength and temperature dependent lineshape parameters of H₂O-, CO₂-, and N₂-perturbed H₂O transitions near 2474 and 2482 nm. *J. Quant. Spectrosc. Radiat. Transf.* **2013**, *130*, 100–111. [[CrossRef](#)]
13. Bendana, F.A.; Lee, D.D.; Schumaker, S.A.; Danczyk, S.A.; Spearrin, R.M. Cross-band infrared laser absorption of carbon monoxide for thermometry and species sensing in high-pressure rocket flows. *Appl. Phys. B* **2019**, *125*, 204. [[CrossRef](#)]
14. Goldenstein, C.S.; Strand, C.L.; Schultz, I.A.; Sun, K.; Jeffries, J.B.; Hanson, R.K. Fitting of calibration-free scanned-wavelength-modulation spectroscopy spectra for determination of gas properties and absorption lineshapes. *Appl. Opt.* **2014**, *53*, 356–367. [[CrossRef](#)]
15. Stewart, G.; Johnstone, W.; Bain, J.; Ruxton, K.; Duffin, K. Recovery of absolute gas absorption line shapes using tunable diode laser spectroscopy with wavelength modulation—Part I: Theoretical analysis. *J. Light. Technol.* **2011**, *29*, 811–821.
16. Li, H.; Rieker, G.B.; Liu, X.; Jeffries, J.B.; Hanson, R.K. Extension of wavelength-modulation spectroscopy to large modulation depth for diode laser absorption measurements in high-pressure gases. *Appl. Opt.* **2006**, *45*, 1052–1061. [[CrossRef](#)]
17. Bain, J.R.P.; Johnstone, W.; Ruxton, K.; Stewart, G.; Lengden, M.; Duffin, K. Recovery of absolute gas absorption line shapes using tunable diode laser spectroscopy with wavelength modulation—Part II: Experimental investigation. *J. Light. Technol.* **2011**, *29*, 987–996. [[CrossRef](#)]
18. Rieker, G.B.; Jeffries, J.B.; Hanson, R.K. Calibration-free wavelength-modulation spectroscopy for measurements of gas temperature and concentration in harsh environments. *Appl. Opt.* **2009**, *48*, 5546. [[CrossRef](#)]
19. Sun, K.; Chao, X.; Sur, R.; Goldenstein, C.S.; Jeffries, J.B.; Hanson, R.K. Analysis of calibration-free wavelength-scanned wavelength modulation spectroscopy for practical gas sensing using tunable diode lasers. *Meas. Sci. Technol.* **2013**, *24*, 125203. [[CrossRef](#)]
20. Neethu, S.; Verma, R.; Kamble, S.S.; Radhakrishnan, J.K.; Krishnapur, P.P.; Padaki, V.C. Validation of wavelength modulation spectroscopy techniques for oxygen concentration measurement. *Sens. Actuators B* **2014**, *192*, 70–76. [[CrossRef](#)]
21. Silver, J.A.; Kane, D.J. Diode laser measurements of concentration and temperature in microgravity combustion. *Meas. Sci. Technol.* **1999**, *10*, 845–852. [[CrossRef](#)]

22. Wei, W.; Chang, J.; Wang, Q.; Qin, Z. Modulation index adjustment for recovery of pure wavelength modulation spectroscopy second harmonic signal waveforms. *Sensors* **2017**, *17*, 163. [[CrossRef](#)] [[PubMed](#)]
23. Wang, B.H.; Jin, Y.; Luo, Y.G. Parametric optimization of eq6110hev hybrid electric bus based on orthogonal experiment design. *Int. J. Automot. Technol.* **2010**, *11*, 119–125. [[CrossRef](#)]
24. Cai, A.H.; Zhou, Y.; Tan, J.Y.; Luo, Y.; Li, T.L.; Chen, M.; An, W.K. Optimization of composition of heat-treated chromium white cast iron casting by phosphate graphite mold. *J. Alloys Compd.* **2008**, *30*, 2339–2344. [[CrossRef](#)]
25. Cai, A.H.; Chen, H.; An, W.K.; Li, X.S.; Zhou, Y. Optimization of composition and technology for phosphate graphite mold. *Mater. Des.* **2008**, *29*, 1835–1839. [[CrossRef](#)]
26. Xia, S.; Lin, R.; Cui, X.; Shan, J. The application of orthogonal test method in the parameters optimization of PEMFC under steady working condition. *Int. J. Hydrogen Energy* **2016**, *41*, 11380–11390. [[CrossRef](#)]
27. Peng, J.; Dong, F.; Xu, Q.; Xu, Y.; Qi, Y.; Xu, H.; Fan, G.; Liu, K. Orthogonal test design for optimization of supercritical fluid extraction of daphnoretin, 7-methoxy-daphnoretin and 1,5-diphenyl-1-pentanone from *stellera chamaejasme* l. and subsequent isolation by high-speed counter-current chromatography. *J. Chromatogr. A* **2006**, *1135*, 151–157. [[CrossRef](#)]
28. Zheng, W.; Dong, J.; Zhang, L.; Chen, Z. Heating performance for a hybrid radiant-convective heating terminal by orthogonal test method. *J. Build. Eng.* **2020**, *33*, 101627. [[CrossRef](#)]
29. Reid, J.; Labrie, D. Second-harmonic detection with tunable diode lasers—Comparison of experiment and theory. *Appl. Phys. B* **1981**, *26*, 203–210. [[CrossRef](#)]
30. Werle, P.; Slemr, F.; Maurer, K.; Kormann, R.; Muecke, R.; Jaenker, B. Near- and mid-infrared laser-optical sensors for gas analysis. *Opt. Lasers Eng.* **2002**, *37*, 101–114. [[CrossRef](#)]
31. Bolshov, M.A.; Kuritsyn, Y.A.; Romanovskii, Y.V. Tunable diode laser spectroscopy as a technique for combustion diagnostics. *Spectrochim. Acta Part B At. Spectrosc.* **2015**, *106*, 45–66. [[CrossRef](#)]
32. Kluczynski, P.; Gustafsson, J.; Lindberg, S.M.; Axner, O. Wavelength modulation absorption spectrometry—An extensive scrutiny of the generation of signals. *Spectrochim. Acta Part B At. Spectrosc.* **2001**, *56*, 1277–1354. [[CrossRef](#)]
33. Gao, X.S.; Zhang, Y.D.; Zhang, H.W.; Wu, Q. Effects of machine tool configuration on its dynamics based on orthogonal experiment method. *Chin. J. Aeronaut.* **2012**, *25*, 285–291. [[CrossRef](#)]
34. Gordon, I.E.; Rothman, L.S.; Hill, C.; Kochanov, R.V.; Tan, Y.; Bernath, P.F.; Birk, M.; Boudon, V.; Campargue, A.; Chance, K.V.; et al. The HITRAN2016 Molecular Spectroscopic Database. *J. Quant. Spectrosc. Radiat. Transf.* **2017**, *203*, 3–69. [[CrossRef](#)]